

Analysis of Bulk Interface Conditions for Atmosphere-Ice-Ocean Coupling

Valentina Schüller^[0000-0002-4579-4217],
Philipp Birken^[0000-0002-6706-3634],
Hanna Kjellson^[0009-0002-1809-0473]

1 Introduction

The atmosphere, ocean, and sea ice components in Earth system models (ESMs) are coupled at the sea surface via boundary conditions. Standard coupling methods correspond to a waveform relaxation (WR) algorithm stopped after one iteration [9]. We are interested in the numerical behavior of this algorithm, in particular how its convergence depends on simulation parameters. For this we propose a coupled toy model that captures the thermodynamics of atmosphere-ice-ocean coupling with *partial* sea ice cover, as typical in ESMs.

This problem can be reduced to coupled heat equations with discontinuous material parameters. There is an existing body of literature on heat equations coupled with Dirichlet-Neumann or Robin-Robin interface boundary conditions. However, the coarse grids used in ESMs directly affect the underlying modeling assumptions and lead to the so-called bulk interface conditions [13]: One requires (a) that the flux across the air-sea interface is continuous and (b) that its magnitude is proportional to the difference in (near-)surface temperatures. The temperature discontinuity is due to the fact that the turbulent surface layers at the interface are unresolved in ESMs. Another consequence of the low resolution is that sea ice covers an *averaged* area fraction of the sea surface, further affecting the interface boundary conditions.

Since bulk interface conditions are specific to ESMs, there are fewer results, but we refer in particular to [2, 5, 13]. In terms of convergence analysis for the corresponding coupling iteration, Clément [2, §6.B] studied a simplified (ice-free) atmosphere-ocean model with bulk interface conditions, discretized in space. Lozano [7] did a continuous convergence analysis for a coupled toy model with a fully ice-covered ocean. Neither of these models reflects the partial sea ice cover typical in ESMs

Valentina Schüller · Philipp Birken · Hanna Kjellson
Lund University, Sweden, e-mail: valentina.schuller@math.lu.se, philipp.birken@math.lu.se,
hanna.kjellson@geol.lu.se

[4, 12]. In this paper, we bridge this gap with the continuous convergence analysis of a coupled ocean-atmosphere model with arbitrary ice cover.

We derive and present the model in the next section and analytically obtain convergence factors of the coupling iteration for the continuous problem in Sec. 3. In Sec. 4, we compare them to a numerical implementation of the same model, allowing us to study the impact of discretization parameters on iteration convergence.

2 Model Derivation

We assume the main thermodynamical process during a typical coupling window $\mathcal{T} \approx 1$ h to be the rapid temperature adjustment in the surface layers due to vertical turbulence. This can be modeled as a diffusive process [2], resulting in two one-dimensional heat equations on $\Omega_O = (h_O, 0)$, $\Omega_A = (0, h_A)$, with $h_O < 0 < h_A$:

$$\begin{aligned} \partial_t T_j - \alpha_j \partial_z^2 T_j &= f_j(t, z) && \text{on } (0, \mathcal{T}] \times \Omega_j, \\ \partial_z T_j(t, z) &= g_j(t) && \text{on } (0, \mathcal{T}] \times \{h_j\}, \\ T_j(0, z) &= \vartheta_j(z) && \text{on } \Omega_j. \end{aligned} \quad (1)$$

The subscript $j \in \{A, O\}$ refers to the atmosphere and ocean, respectively. We denote source terms by $f_j(t, z)$, boundary data by $g_j(t)$, initial data by $\vartheta_j(z)$, and the diffusivity by α_j , cf. Fig. 1 (left).

The equations are coupled at the sea surface Γ , where $z = 0$. Without sea ice, one uses bulk interface conditions, which follow from linearizing the so-called law of the wall. They consist of a Robin and a Neumann condition:

$$\begin{aligned} k_A \partial_z T_A|_{\Gamma} &= C_{AO} (T_A|_{\Gamma} - T_O|_{\Gamma}) =: \mathcal{J}_{AO}, \\ k_O \partial_z T_O|_{\Gamma} &= k_A \partial_z T_A|_{\Gamma}, \end{aligned}$$

with bulk coefficient C_{AO} . Notably, they allow for a temperature jump across Γ .

Sea ice takes up an averaged area fraction $a_I \in [0, 1]$ of Γ and affects the boundary condition seen by the atmosphere and ocean models:

$$\begin{aligned} k_A \partial_z T_A|_{\Gamma} &= a_I \mathcal{J}_{AI} + (1 - a_I) \mathcal{J}_{AO}, \\ k_O \partial_z T_O|_{\Gamma} &= a_I \mathcal{J}_{IO} + (1 - a_I) \mathcal{J}_{AO}. \end{aligned} \quad (2)$$

The atmosphere-ice and ice-ocean fluxes depend on the sea ice surface and bottom temperatures $T_{I,s}$ and $T_{I,b}$, respectively:

$$\mathcal{J}_{AI} = C_{AI} (T_A|_{\Gamma} - T_{I,s}), \quad \mathcal{J}_{IO} = C_{IO} (T_{I,b} - T_O|_{\Gamma}). \quad (3)$$

See Fig. 1 for a depiction of this problem setup.

$T_{I,s}$ and $T_{I,b}$ are provided by a simplified sea ice model based on [10, App. A]. The latter is constant and equal to the freezing temperature of seawater. $T_{I,s}$ is computed

from a surface energy balance: Its value is at most 0°C and such that the conductive heat flux inside ice is in balance with the net surface heat flux over ice:

$$T_{I,s} = \min \left\{ \frac{\frac{k_I}{h_I(t)} T_{I,b} + R + C_{AI} T_A|_\Gamma}{k_I/h_I(t) + B + C_{AI}}, 0^\circ\text{C} \right\}. \quad (4)$$

Therein, the constants k_I and R are the thermal conductivity of ice and incoming radiation. B results from a linear approximation of the Stefan-Boltzmann law [11].

Ice thickness $h_I(t)$ evolves as a result of vertical growth and melt processes [10, 11], due to surplus heat at the surface and the turbulent heat flux below sea ice:

$$-q_I \frac{dh_I}{dt} = R - BT_{I,s} + \mathcal{J}_{AI}(T_A, T_{I,s}) - \mathcal{J}_{IO}(T_O), \quad (5)$$

wherein q_I is the latent heat of fusion. This process makes the model nonlinear (a special case of the Chini equation [7]).

We now study the following sequential coupling iteration for the coupled toy model that results from Eqs. (1–5): Given initial guesses $T_O^0, T_{I,s}^0$, compute for $k = 1, 2, \dots$

$$\begin{aligned} \partial_t T_A^k - \alpha_A \partial_z^2 T_A^k &= f_A \quad \text{on } (0, \mathcal{T}] \times \Omega_A, \\ k_A \partial_z T_A^k|_\Gamma &= a_I C_{AI} (T_A^k|_\Gamma - T_{I,s}^{k-1}) + (1 - a_I) C_{AO} (T_A^k|_\Gamma - T_O^{k-1}|_\Gamma), \end{aligned} \quad (6a)$$

followed by

$$\begin{aligned} -q_I \frac{dh_I^k}{dt} &= R - BT_{I,s}^k + C_{AI} (T_A^k|_\Gamma - T_{I,s}^k) + C_{IO} (T_O^{k-1}|_\Gamma - T_{I,b}), \\ T_{I,s}^k &= \min \left\{ \frac{\frac{k_I}{h_I^k} T_{I,b} + R + C_{AI} T_A^k|_\Gamma}{k_I/h_I^k + B + C_{AI}}, 0^\circ\text{C} \right\}, \end{aligned} \quad (6b)$$

and

$$\begin{aligned} \partial_t T_O^k - \alpha_O \partial_z^2 T_O^k &= f_O \quad \text{on } (0, \mathcal{T}] \times \Omega_O, \\ k_O \partial_z T_O^k|_\Gamma &= a_I C_{IO} (T_{I,b} - T_O^k|_\Gamma) + (1 - a_I) k_A \partial_z T_A^k|_\Gamma, \end{aligned} \quad (6c)$$

with initial data $T_j^k(0, z) = \vartheta_j(z)$, $h_I^k(0) = h_0$, and boundary data $\partial_z T_j^k(t, h_j) = g_j(t)$, $j \in \{A, O\}$. Using the flux $k_A \partial_z T_A^k|_\Gamma$ in Eq. (6c) (and not $T_A^k|_\Gamma$) ensures air-sea flux conservation in every iteration.

3 Linear Convergence Analysis of the Coupling Iteration

In this section, we derive the main analysis result for the iteration (6). We study the decay of the coupling error in iteration k at the interface Γ ,

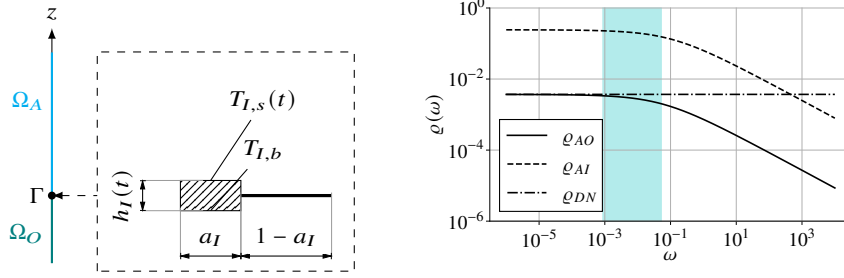


Fig. 1 Left: Sea ice has an area fraction a_I and thickness $h_I(t)$ on Γ . Right: Comparison of analytically derived convergence factors.

$$e_j^k(t, z) := T_j^k(t, z) - T_j(t, z),$$

where j can be A , O , or I,s . For linear iterations and infinitely large time windows $\mathcal{T} = \infty$, one can use the technique from, e.g., [3] to study the convergence factor in Fourier space, i.e.,

$$\varrho(\omega) := \left| \frac{\hat{e}_A^k(\omega, 0)}{\hat{e}_A^{k-1}(\omega, 0)} \right|, \quad \omega \in \mathbb{R}, \quad (7)$$

where $\hat{e}_j^k(\omega, z)$ denotes the Fourier transform in time of $e_j^k(t, z)$, assuming vanishing Fourier coefficients for $t < 0$. It is the same in all three subdomains and independent of k .

Since the ice model (6b) is nonlinear, we consider a linearized version for the analysis. By assuming $\frac{d}{dt}h_I \ll h_I$ during a coupling window, i.e., $h_I(t) \approx h_0$, as well as $T_{I,s} < 0^\circ\text{C}$, the new ice model reads:

$$T_{I,s}^k = \frac{R + C_{AI} T_A^k|_\Gamma + \frac{k_I}{h_0} T_{I,b}}{\frac{k_I}{h_0} + B + C_{AI}}. \quad (8)$$

In particular, note that $\hat{e}_{I,s}^k = C_{AI}/(k_I/h_0 + B + C_{AI}) \hat{e}_A^k|_\Gamma$.

Theorem 1 *The convergence factor of the iteration (6) with linearized ice model (8) for $\mathcal{T} = \infty$ is given by*

$$\varrho(\omega) = \frac{\left| a_I C_{AI} \zeta + (1 - a_I)^2 C_{AO} \frac{\frac{k_A}{\sqrt{\alpha_A}} \sqrt{i\omega} \tanh(\xi_A \sqrt{i\omega})}{\frac{k_O}{\sqrt{\alpha_O}} \sqrt{i\omega} \tanh(\xi_O \sqrt{i\omega}) - a_I C_{IO}} \right|}{\left| \frac{k_A}{\sqrt{\alpha_A}} \sqrt{i\omega} \tanh(\xi_A \sqrt{i\omega}) + a_I C_{AI} + (1 - a_I) C_{AO} \right|}, \quad (9)$$

where

$$\zeta := \frac{C_{AI}}{\frac{k_I}{h_0} + B + C_{AI}}, \quad \xi_A := \frac{h_A}{\sqrt{\alpha_A}}, \quad \xi_O := \frac{h_O}{\sqrt{\alpha_O}}.$$

For $a_I = 0, a_I = 1$, we immediately obtain the following corollary:

Corollary 1 *The convergence factors for ice-free and fully ice-covered conditions are given by*

$$\varrho_{AO}(\omega) = \frac{k_A}{k_O} \sqrt{\frac{\alpha_O}{\alpha_A}} \left| \frac{\tanh(\xi_A \sqrt{i\omega})}{\tanh(\xi_O \sqrt{i\omega})} \right| \frac{1}{\left| \frac{k_A \sqrt{i\omega}}{C_{AO} \sqrt{\alpha_A}} \tanh(\xi_A \sqrt{i\omega}) + 1 \right|} \quad (10)$$

and

$$\varrho_{AI}(\omega) = \frac{\zeta}{\left| 1 + \frac{k_A \sqrt{i\omega}}{C_{AI} \sqrt{\alpha_A}} \tanh(\xi_A \sqrt{i\omega}) \right|}, \quad (11)$$

respectively.

Proof (Theorem 1). We study the coupling iteration of $\hat{e}_j^k(\omega, z)$. By the Fourier transform, we obtain from (6) and (8) that, given \hat{e}_j^0 , we have for $k = 1, 2, \dots$:

$$\begin{aligned} i\omega \hat{e}_A^k - \alpha_A \partial_z^2 \hat{e}_A^k &= 0, \\ k_A \partial_z \hat{e}_A^k|_{\Gamma} &= a_I C_{AI} \left(\hat{e}_A^k|_{\Gamma} - \zeta \hat{e}_A^{k-1}|_{\Gamma} \right) + (1 - a_I) C_{AO} \left(\hat{e}_A^k|_{\Gamma} - \hat{e}_O^{k-1}|_{\Gamma} \right), \end{aligned}$$

and

$$\begin{aligned} i\omega \hat{e}_O^k - \alpha_O \partial_z^2 \hat{e}_O^k &= 0, \\ k_O \partial_z \hat{e}_O^k|_{\Gamma} &= -a_I C_{IO} \hat{e}_O^k|_{\Gamma} + (1 - a_I) k_A \partial_z \hat{e}_A^k|_{\Gamma}, \end{aligned}$$

with homogeneous initial conditions and boundary data on h_A, h_O .

A standard solution ansatz for the differential equations with boundary data at h_j yields

$$\hat{e}_j^k(\omega, z) = \beta_j^k(\omega) \cosh\left((h_j - z)\sqrt{i\omega/\alpha_j}\right).$$

with iteration-dependent coefficients $\beta_j^k(\omega)$. The convergence factor in Fourier space (7) thus reduces to:

$$\varrho(\omega) = \left| \frac{\hat{e}_A^k(\omega, 0)}{\hat{e}_A^{k-1}(\omega, 0)} \right| = \left| \frac{\beta_A^k(\omega)}{\beta_A^{k-1}(\omega)} \right|.$$

We obtain $\beta_A^k(\omega)$ and $\beta_O^k(\omega)$ from the interface boundary conditions (2):

$$\begin{aligned} \beta_A^k(\omega) &= \frac{\beta_A^{k-1}(\omega) a_I C_{AI} \zeta \cosh(\xi_A \sqrt{i\omega}) + \beta_O^{k-1} (1 - a_I) C_{AO} \cosh(\xi_O \sqrt{i\omega})}{\frac{k_A}{\sqrt{\alpha_A}} \sqrt{i\omega} \sinh(\xi_A \sqrt{i\omega}) + (a_I C_{AI} + (1 - a_I) C_{AO}) \cosh(\xi_A \sqrt{i\omega})}, \\ \beta_O^k(\omega) &= \beta_A^k(\omega) \frac{(1 - a_I) \frac{k_A}{\sqrt{\alpha_A}} \sqrt{i\omega} \sinh(\xi_A \sqrt{i\omega})}{\frac{k_O}{\sqrt{\alpha_O}} \sqrt{i\omega} \sinh(\xi_O \sqrt{i\omega}) - a_I C_{IO} \cosh(\xi_O \sqrt{i\omega})}. \end{aligned}$$

Inserting the second equation in the first and dividing by β_A^{k-1} gives the result. \square

Table 1 Parameter values used for numerical examples.

	Atm.	Oce.	Ice	Parameter	Value
h [m]	200	-50	1	C_{AO}	1.3
α [$\text{m}^2 \text{s}^{-1}$]	1.92×10^{-5}	1.39×10^{-7}	—	C_{AI}	1.82
k [J/Kms]	2.4×10^{-2}	0.57	2.03	B	$3.62 \text{ J/m}^2 \text{ s}^\circ\text{C}$
Δt [s]	60	600	600	\mathcal{T}	3600 s
Δz [m]	1	1	—		

Remark 1 In case of a fully ice-covered ocean ($a_I = 1$), $e_O^k(\omega, z) \equiv 0$. This directly follows from the fact that the sea ice bottom temperature $T_{I,b}$ is independent of k .

Remark 2 If we consider the same model problem in ice-free conditions ($a_I = 0$), but with Dirichlet-Neumann conditions at the interface, i.e.,

$$T_A^k|_\Gamma = T_O^{k-1}|_\Gamma, \quad k_O \partial_z T_O^k|_\Gamma = k_A \partial_z T_A^k|_\Gamma,$$

the convergence factor is given by [2]

$$\varrho_{DN}(\omega) = \frac{k_A}{k_O} \sqrt{\frac{\alpha_O}{\alpha_A}} \left| \frac{\tanh(\xi_A \sqrt{i\omega})}{\tanh(\xi_O \sqrt{i\omega})} \right|. \quad (13)$$

Fig. 1 shows ϱ_{AO} , ϱ_{AI} , ϱ_{DN} over a range of frequencies ω using typical parameters, cf. Tab. 1. In practice, $\tanh(\xi_j \sqrt{i\omega}) \approx \pm 1$ and thus $\varrho_{DN} \approx k_A \sqrt{\alpha_O} / (k_O \sqrt{\alpha_A})$ near-constant. For low frequencies, $\varrho_{AO} \approx \varrho_{DN}$ (i.e., it is mostly independent of C_{AO}) and $\varrho_{AI} \approx \zeta$ (which depends on C_{AI}). Note in particular that $\zeta > \varrho_{DN}$. The additional $1/\sqrt{i\omega}$ terms in ϱ_{AO} and ϱ_{AI} manifest as a decay for high frequencies.

To estimate convergence in numerical simulations, we consider the range of frequencies resolved after time discretization [3, 6]. Assuming a minimum solver time step size of 60 s and a coupling window size $\mathcal{T} = 1$ h, one obtains the frequency band $[\omega_{\min}, \omega_{\max}] = [\frac{\pi}{1\text{h}}, \frac{\pi}{60\text{s}}]$, shaded in blue in Fig. 1. In this range, $\varrho_{AO} \approx \varrho_{DN}$ and $\varrho_{AI} \approx \zeta$.

4 Numerical Experiments

We now compare the continuous analysis results with a numerical implementation of the iteration (6), with implementation choices motivated by the state of the art in ESMs. One is free to pick discretization methods and grid sizes suitable for the relevant physical scales in each component. We discretize all components using cell-centered finite differences in space [5, Fig. 1b] and the implicit Euler method in time. Components exchange boundary data averaged over the coupling window $[0, \mathcal{T}]$ (see [5] for a motivation). The simulation parameters are standard for climate

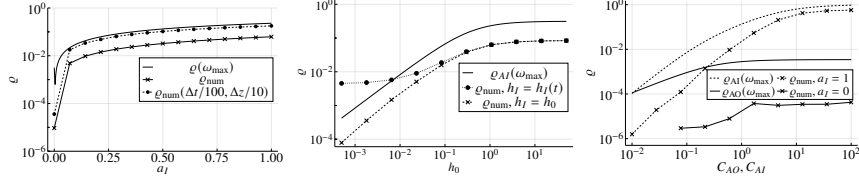


Fig. 2 Dependence of the analytical and numerical convergence factors on ice area fraction (left), ice thickness (middle), and bulk coefficients (right).

applications [7, 9] and given in Tab. 1. Our code is based on the open-source coupling software `ClimaCoupler.jl` [1] and available at [8].

We compute the numerical convergence factor based on atmospheric data,

$$\varrho_{\text{num}} = \frac{\|T_{A,\Gamma}^k - T_{A,\Gamma}^{K-1}\|_2}{\|T_{A,\Gamma}^{k-1} - T_{A,\Gamma}^{K-1}\|_2}, \quad T_A^k \in \mathbb{R}^{N_A},$$

where $N_A = \mathcal{T}/\Delta t_A$ is the number of time steps during a coupling window and K is large enough to achieve convergence up to floating-point precision.

In Fig. 2 we compare the analytical and numerical convergence factors for varying ice area fraction a_I , initial ice thickness h_0 , and bulk coefficients C_{AI} , C_{AO} . Since the analytical convergence factor ϱ decreases monotonously in the resolved frequency band, we choose to evaluate it at $\omega_{\min} = \pi/\mathcal{T}$ for the comparison. Much of the numerically observed convergence behavior can be explained from the continuous estimate, in particular the increase in ϱ_{num} for larger values of all investigated parameters. Note however that the continuous factor tends to be larger than ϱ_{num} . The difference is partly due to the coarse discretization: In the leftmost plot, we include a result with reduced grid sizes ($\Delta t/100$, $\Delta z/10$) to illustrate this. The disagreement is smaller for $a_I \neq 0$, which might be related to the lack of space discretization (errors) in the ice model. For thin ice, the analysis result does not match the numerical behavior; this is due to the linearization (8) where we assumed $\frac{d}{dt}h_I \ll h_I$. They agree much better if the code uses the linear ice model (8).

5 Conclusion

We have presented a continuous WR convergence analysis for a toy model of thermodynamical atmosphere-ice-ocean coupling. Coarse discretizations in climate codes affect the underlying model equations; we focus here on bulk interface conditions and partial sea ice cover. They lead to qualitative differences in the convergence results compared to standard conjugate heat transfer problems. Compared to Dirichlet-Neumann WR, the analysis of bulk interface conditions yields a decay of the convergence factor for high frequencies. Convergence of the iteration depends on the ice area fraction nonlinearly. Numerical results illustrate the latter and show how

the nonlinear ice thickness feedback and coarse grids further affect observed WR convergence.

Acknowledgements The research presented in this paper is a contribution to the Strategic Research Area “Modelling the Regional and Global Earth system”, MERGE, funded by the Swedish government.

References

1. ClimaCoupler.jl (2025). URL <https://github.com/CliMA/ClimaCoupler.jl>
2. Clément, S.: Numerical analysis for a combined space-time discretization of air-sea exchanges and their parameterizations. Ph.D. thesis, Université Grenoble Alpes (2022)
3. Gander, M.J., Halpern, L.: Optimized Schwarz waveform relaxation methods for advection reaction diffusion problems. *SIAM J. Numer. Anal.* **45**(2), 666–697 (2007)
4. Hunke, E., et al.: CICE-Consortium/Icepack: Icepack 1.5.0. Zenodo (2024). DOI 10.5281/zenodo.14188409
5. Lemarié, F., Blayo, E., Debreu, L.: Analysis of ocean-atmosphere coupling algorithms: Consistency and stability. *Procedia Comput. Sci.* **51**, 2066–2075 (2015). DOI 10.1016/j.procs.2015.05.473
6. Lemarié, F., Debreu, L., Blayo, E.: Toward an optimized global-in-time Schwarz algorithm for diffusion equations with discontinuous and spatially variable coefficients, Part I: The constant coefficients case. *Electron. Trans. Numer. Anal.* **40**, 148–169 (2013)
7. Lozano, P.: Analysis and optimization of Schwarz algorithms for ocean-sea ice-atmosphere coupling. MS Thesis, Université Grenoble Alpes, Grenoble, France (2022)
8. Schüller, V., Kjellson, H.: Toy examples for ClimaCoupler.jl. Zenodo (2025). DOI 10.5281/ZENODO.17222379
9. Schüller, V., Lemarié, F., Birken, P., Blayo, E.: Quantifying coupling errors in atmosphere-ocean-sea ice models: A study of iterative and non-iterative approaches in the EC-Earth AOSCM. *Geosci. Model Dev.* **18**(22), 9167–9187 (2025). DOI 10.5194/gmd-18-9167-2025
10. Semtner, A.J.: A model for the thermodynamic growth of sea ice in numerical investigations of climate. *J. Phys. Oceanogr.* **6**(3), 379–389 (1976)
11. Thorndike, A.S.: A toy model linking atmospheric thermal radiation and sea ice growth. *J. Geophys. Res. C: Oceans* **97**(C6), 9401–9410 (1992). DOI 10.1029/92JC00695
12. Vancoppenolle, M., et al.: SI3, the NEMO sea ice engine (2023). DOI 10.5281/zenodo.7534900
13. Zhang, H., Liu, Z., Constantinescu, E., Jacob, R.: Stability analysis of interface conditions for ocean-atmosphere coupling. *J. Sci. Comput.* **84**(3), 44 (2020). DOI 10.1007/s10915-020-01293-y